JOURNAL OF GUIDANCE, CONTROL, AND DYNAMICS
Vol. 18, No. 2, March–April 1995

Attitude Control System Conceptual Design for Geostationary Operational Environmental Satellite Spacecraft Series

F. L. Markley,* F. H. Bauer,† J. J. Deily,‡ and M. D. Femiano‡
NASA Goddard Space Flight Center, Greenbelt, Maryland, 20771

The next generation of the Geostationary Operational Environmental Satellite (GOES-N) will require extremely stringent pointing performance for improved weather prediction. These spacecraft will employ high-precision gyros and star trackers in a unique control system design concept to achieve the end-to-end pointing performance at the focal plane of the instruments. This paper presents the GOES-N attitude control system conceptual design, sensor complement trade-offs, attitude determination theory, and system performance expectations.

Introduction

SEVERAL near-Earth spacecraft have employed attitude determination and control systems using gyro and star tracker data processed by Kalman filtering algorithms,[1–4] but this form of attitude determination and control has not been commonly employed for geostationary spacecraft. The next generation of the Geostationary Operational Environmental Satellite (GOES-N) has extremely stringent pointing requirements, 33 μrad absolute pointing and 14 μrad within-frame and frame-to-frame jitter stability (per axis, 3σ), for which a gyro/star tracker system is well suited. The proposed GOES-N spacecraft configuration is shown in Fig. 1. There are two alternate instrument designs; one uses passive cooling for the infrared focal plane and requires a semiannual 180 deg yaw maneuver to keep sunlight out of the coolers, whereas the other employs active cooling and does not require the yaw maneuver.

The actual pointing requirement for GOES-N is at the focal plane of the spacecraft instruments, the imager and sounder. The end-to-end system performance for GOES-N relies on the arcsecond pointing determination of the star tracker/gyro system to generate error signals in roll, pitch, and yaw. The error signals are processed in the attitude control electronics to produce two sets of control signals: low-frequency (about 0.1-Hz-bandwidth) signals to maintain spacecraft pointing by reaction wheel control and high-frequency signals for repointing the instrument mirrors to compensate for the attitude errors that the closed-loop reaction wheel control cannot follow. This mirror control, termed spacecraft motion compensation, compensates for disturbances in a midrange of frequencies above the spacecraft controller bandwidth and below the frequency levels that the spacecraft will not respond to significantly, chiefly those contributed by the instrument scanning mirrors.

In comparison with conventional geostationary momentum bias Earth sensor-based controllers such as those planned for the GOES-I spacecraft, the GOES-N control system provides a significant improvement in system performance owing to active three-axis control with wider bandwidth to better track perturbations, rapid recovery within minutes following a stationkeeping maneuver, lower jitter, immunity to Earth clouds and Earth radiance gradients, and real-time repointing of the mirrors based on error signals rather than models to compensate for dynamic interactions. This paper presents the attitude determination sensing and processing, including the trade-offs considered in choosing the sensor complement, the spacecraft attitude control algorithms, the spacecraft motion compensation concept, and the GOES-N simulation results.

Attitude Determination

Inertial Reference Units

The sensor configurations studied include an accurate inertial reference unit, or gyro package, that provides complete rotational rate information on the three spacecraft axes. This information is available for spacecraft attitude control in the normal mission mode and for rapid recovery from the attitude disturbances caused by stationkeeping maneuvers (typically in 5–10 min rather than the 5–10 h required for the GOES-I configuration). The gyro outputs are also employed for spacecraft motion compensation, the real-time commanding of the instrument mirror gimbal drives to compensate for spacecraft attitude disturbances.

The baselined inertial reference unit is the Dry Rotor Inertial Reference Unit (DRIRU-II), a fully redundant package including three dry-tuned two-axis gyros and associated electronics. There is extensive flight experience with this unit, including Solar Maximum Mission , Landsats 4 and 5, the Upper Atmosphere Research Satellite, the Extreme Ultraviolet Explorer, the Compton Gamma Ray Observatory, ETS-1, and at least two Department of Defense missions. Only one inflight failure has been experienced, an electronic (not mechanical) failure of one of the six output channels on Solar Maximum Mission. The DRIRU-II has excellent drift and noise characteristics, characterized by drift rate stability of 0.0145 μrad/s/6 h, rate white noise of 0.206 μrad/s$^{1/2}$, and rate random walk of 2.15×10^{-4} μrad/s$^{3/2}$. These values were based on 50 h of gyro rate data taken for an Advanced X-ray Astronomy Facility fine pointing study in 1988 and represent extremely low noise gyros, probably the best of the SDG-5 gyros used in DRIRU-II. Alternative gyros such as hemispherical resonator gyros, fiberoptic gyros, or ring laser gyros have potential payoffs in lower power or weight or increased lifetime, but they have little flight experience and therefore higher risk.

Attitude References

No further sensing would be necessary if the gyros were perfect, but additional attitude sensors are required to compensate for the inevitable gyro drifts. The information from these sensors can be optimally combined with the gyro data using an extended Kalman filter.[1,4] The traditional attitude references for fine pointing missions have been provided by star trackers. This technology is quite mature and has been used on several NASA missions including Landsats 4 and 5, Compton Gamma Ray Observatory, Upper Atmosphere Research Satellite, and Extreme Ultraviolet Explorer.

A gyro–star tracker attitude system provides an attitude referenced to inertial space, as defined by the fixed stars. Thus an in-track or cross-track error in spacecraft location results in a 1 : 1 error in

Presented as Paper 91-2832 at the AIAA Guidance, Navigation, and Control Conference, New Orleans, LA, Aug. 12–14, 1991; received March 6, 1992; revision received July 20, 1994; accepted for publication July 20, 1994.

*Aerospace Engineer, Guidance and Control Branch, Code 712. Associate Fellow AIAA.

†Head, Guidance and Control Branch, Code 712. Senior Member AIAA.

‡Aerospace Engineer, Guidance and Control Branch, Code 712. Member AIAA.

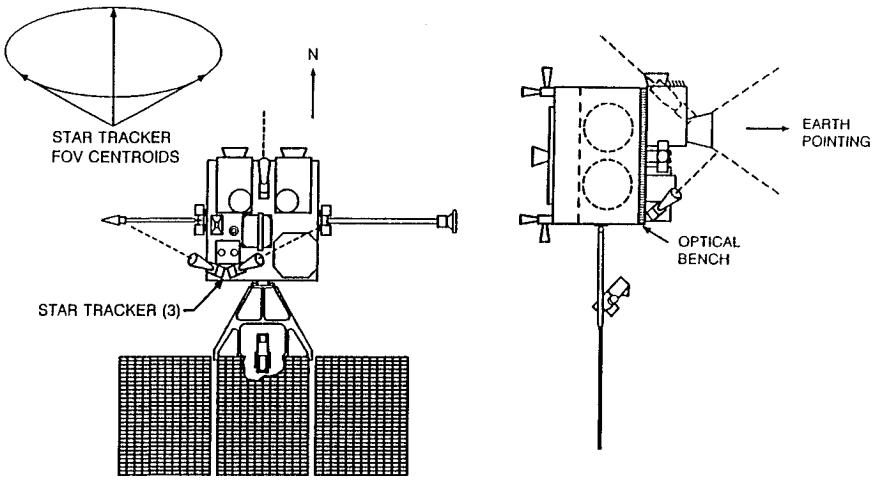

Fig. 1 GOES-N spacecraft configuration.

the registration of a pixel in an instrument field of view relative to a fixed grid on Earth. It would be preferable to have an Earth-referenced attitude keeping the spacecraft z axis nadir pointing so that the registration error resulting from an in-track or cross-track ephemeris error would be reduced by the ratio of Earth's equatorial radius to the spacecraft orbit radius, $6378/42164 = 0.15$. Beacons and landmarks were investigated in an effort to achieve this 85% reduction in the effect of ephemeris errors but were rejected as impractical.[5] Infrared Earth sensors were not considered because of their sensitivity to cold clouds and radiance gradients.

Star Trackers

The proposed GOES-N attitude control system includes three fixed-head star trackers. Two star trackers are needed for accurate attitude determination, since a single star tracker provides very poor information about rotations around its boresight. The principal reason for including the third tracker is redundancy, but performance is improved if all three star trackers are employed simultaneously. The trackers must be oriented so that their fields of view are shielded from interference by the sun, moon, and Earth. The sun, being the brightest of these objects, constitutes the most significant problem. A reasonable requirement for a sunshield is to allow star tracker operation except when the sun is within 30 deg of the star tracker boresight. Since the sun is never farther than 23.44 deg from Earth's equatorial plane, orienting the star tracker boresights at 35 deg from the north or south pole will avoid sun interference completely. Earth and moon interference are also avoided by this configuration. The baselined GOES-N configuration has the tracker boresights equally spaced in azimuth at an angle of 35 deg from the spacecraft $-y$ (negative pitch) axis, as shown in Fig. 1. The north face is chosen to avoid interference by reflections from the solar array; deletion of the GOES-I solar sail from this face is quite desirable to avoid interference with the star tracker.

At least two charge-coupled device (CCD) star trackers have been designed as replacements for the NASA Standard Star Tracker, which uses an image dissector tube rather than a solid-state focal plane detector.[6–8] They have 8 deg square fields of view, can simultaneously track up to five stars as dim as sixth magnitude, have noise equivalent angles of 8 μrad, weigh less than 9 kg, and require less than 15 W of power. The limiting parameter for star tracker performance may be calibration error rather than noise, since calibration to better than 1 arcsec (4.8 μrad) is beyond current capabilities, owing to atmospheric effects in ground testing, limitations of collimated light sources, etc. This calibration error includes a constant component and a component that varies over the tracker field of view. The former can be removed by ground-based in-flight calibration, whereas the latter will tend to average out if several stars are observed simultaneously.

There are approximately four times as many stars per unit solid angle near the galactic equator than there are near the galactic poles, which are at declination 27.4 deg, right ascension 192.25 deg, and declination -27.4 deg, right ascension 12.25 deg in Earth-centered inertial coordinates. It is important to note that at most one of the three tracker fields of view, in the configuration of Fig. 1, can be located closer than 30 deg from a galactic pole at any time. The probability $P(n)$ of having n stars in the field of view follows a Poisson distribution

$$P(n) = \exp(-n_{\text{ave}})(n_{\text{ave}})^n/n! \tag{1}$$

where n_{ave} is the average number of stars in the field of view, which depends on both the size of the field of view and the tracker sensitivity. Analysis shows that two of three star trackers with an 8 deg square field of view and sensitivity to magnitude 6.0 will almost certainly have five or more stars in their fields of view, whereas the third will very probably have three or more.[5]

An advantage of having the three star tracker boresights at equal angles to the pitch axis is that the tracker fields of view will sweep out the same band in the celestial sphere as the spacecraft rotates during its 24-h orbit, so that the three trackers can share a common star catalog. The size of the catalog depends on both the minimum magnitude of stars included and the size of the star tracker field of view. An estimate of the size of the onboard star catalog required is given by

$$n_{\text{cat}} = n_{\text{ave}} \times (360 \text{ deg}) \times \sin(35 \text{ deg})/d \tag{2}$$

where d is the length of a side of the tracker field of view in degrees. The average density over the celestial sphere is about three-fourths of the density at the galactic equator,[6] which gives a catalog size of 620 stars for the star tracker parameters discussed above. If a 180-deg yaw maneuver is performed semiannually, then two catalogs of this size are required, one for each yaw attitude. Either they can be simultaneously resident in the onboard computer memory or else the catalog can be reloaded at the time of the yaw maneuver. The above estimates must be verified by detailed simulations using real star catalogs, but the results should differ only in detail. The assessment of the location errors of stars in actual catalogs will also be necessary. For this study, it suffices to note that there is a catalog of International Reference Stars, uniformly distributed at one star per square degree over the celestial sphere, with location errors of 1.5 μrad or less. These reference stars have magnitudes between 7.5 and 10.5, and it is generally true that the locations of brighter stars are better known than those of dimmer stars.

Kalman Filter

In order to accurately estimate the spacecraft attitude, the sensor data from the gyro and star trackers described above must be processed in an onboard computer using an extended Kalman filter attitude estimation algorithm.[1,4] The vehicle three-axis attitude is maintained in the flight computer as a quaternion q. The output gyro rate data is sampled every T_g seconds (where T_g is typically equal

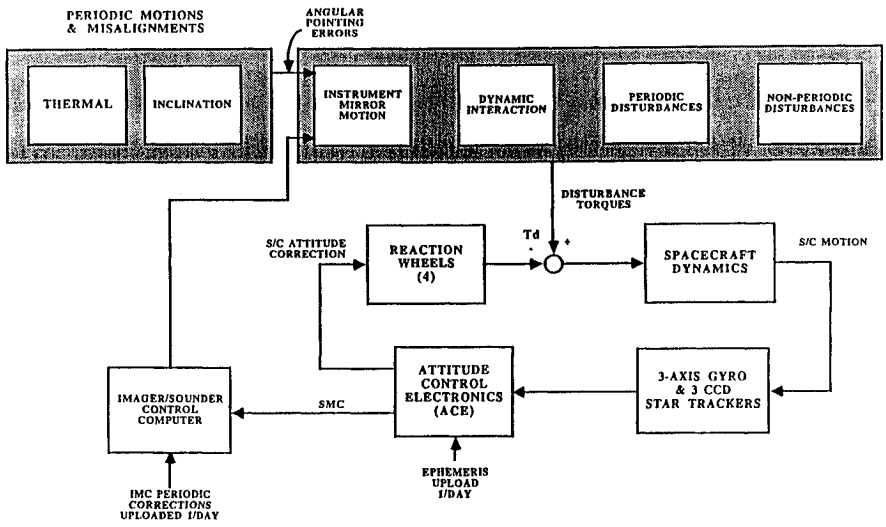

Fig. 2 Attitude control system.

to 0.1 s, the value assumed here for GOES-N), processed to remove the estimated drift rate bias, and used to propagate the quaternion q. At an update period T, which is some multiple of T_g, the star tracker measurements are used to optimally compute a six-component state vector comprising the errors in the three estimated gyro drift rate biases and three attitude error angles. The Kalman filter outputs are then used to update the inertial attitude quaternion q and the three gyro biases.

The predicted performance of the attitude estimation can be found by numerically iterating the Kalman filter equations to steady state, but Farrenkopf[9] obtained analytic solutions for the case when the three attitude error angles can be assumed to be uncoupled. The gyro noise model is[1,4,9,10]

$$\frac{d\theta}{dt} = \omega + n_v + b \tag{3}$$

$$\frac{db}{dt} = n_u \tag{4}$$

where θ is the gyro output angle, ω is the true angular rate about the gyro input axis, b is the gyro drift rate, and n_u and n_v are Gaussian-distributed zero-mean white-noise sources. The process n_v models the instantaneous rate white noise with standard deviation σ_v, whereas n_u accounts for the long-term drift rate variation as a random walk (an integrated white-noise process with standard deviation σ_u). The star tracker noise n_T is modeled as white, Gaussian, and zero mean with standard deviation σ_n.

Farrenkopf's results for the preupdate and postupdate attitude error standard deviations, denoted by $\sigma(-)$ and $\sigma(+)$, respectively, can be written as

$$\sigma(-) = \sigma_n(\xi^2 - 1)^{\frac{1}{2}} \tag{5}$$

$$\sigma(+) = \sigma(-)/\xi \tag{6}$$

where

$$\xi = \tfrac{1}{2}\left[\gamma + \tfrac{1}{2}S_u + \left(\gamma S_u + S_v^2 + \tfrac{1}{3}S_u^2\right)^{\frac{1}{2}}\right] \tag{7}$$

$$\gamma = \left[4 + S_v^2 + (1/12)S_u^2\right]^{\frac{1}{2}} \tag{8}$$

$$S_u = \sigma_u T^{\frac{3}{2}}/\sigma_n \tag{9}$$

$$S_v = \sigma_v T^{\frac{1}{2}}/\sigma_n \tag{10}$$

In the limiting case of very frequent updates, the preupdate and postupdate attitude error standard deviations both approach the continuous-update limit

$$\sigma_c = T^{\frac{1}{4}}\sigma_n^{\frac{1}{2}}\left(\sigma_v^2 + 2\sigma_u\sigma_n T^{\frac{1}{2}}\right)^{\frac{1}{4}} \tag{11}$$

Table 1 Single-axis estimation errors for different update times

Update time, s	$\sigma(-)$, μrad	$\sigma(+)$, μrad	σ_c, μrad
1.0	1.03	1.02	1.01
2.0	1.25	1.21	1.21
10.0	1.97	1.83	1.84
100.0	4.29	3.21	3.49

Assuming the gyro standard deviations σ_u and σ_v given above for the DRIRU-II and setting σ_n to 4.8 μrad, corresponding to the estimated best calibration accuracy of 1 arcsec (which, however, is not really a source of Gaussian noise), give the standard deviations as functions of the update time T shown in Table 1. In all but the 100-s update cases, the continuous-update limit gives a reasonably accurate and relatively simple estimate of the attitude estimation errors. The even simpler limiting form

$$\sigma_c = T^{\frac{1}{4}}\sigma_n^{\frac{1}{2}}\sigma_v^{\frac{1}{2}} \tag{12}$$

is valid when the contribution of σ_u to the attitude estimation errors is negligible; it shows a one-half power dependence on both σ_v and σ_n and a one-fourth power law dependence on the update time T. This shows why it is extremely difficult to improve the attitude determination performance by increasing the update frequency.

These analytic results are strictly true only if all the star observations are at the same point in the star tracker field of view, and the resulting error estimates are for rotation errors about the two axes perpendicular to the line of sight to the star; the errors for rotations about the line of sight are infinite. The results are quite accurate for a single small-field-of-view star tracker, with effectively infinite attitude uncertainties for rotations about the tracker boresight. The results for several trackers can be obtained by adding the information (inverse variance) obtained by the different trackers, but this will not be pursued further, since the simulation described below gives these results. The purpose of the analysis of this section is to provide order-of-magnitude estimates that establish the validity of the gyro–star tracker system and justify its further study.

Control System and Control Processor Design

Baseline Controller Overview

The spacecraft attitude and rates are sensed by the fully redundant gyro–star tracker–reaction wheel system described above. The control signals are based on the difference between these sensed values and the commanded attitude and rates (Fig. 2). The commanded inertial attitude matrix has rows that are related to the spacecraft

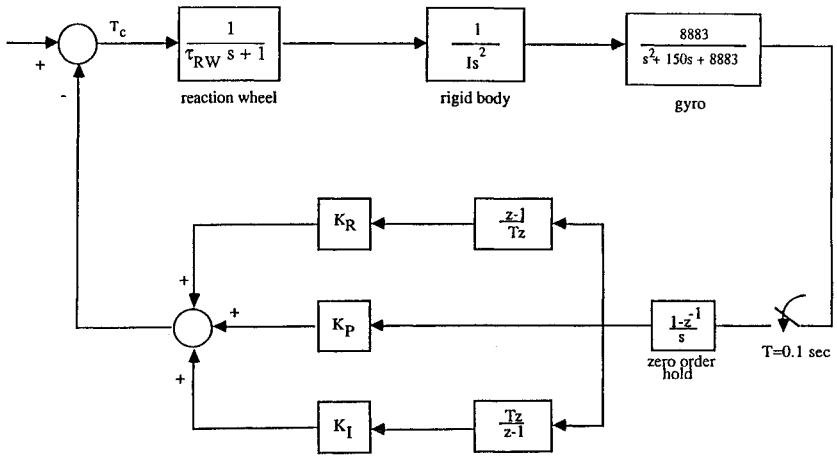

Fig. 3 PID controller.

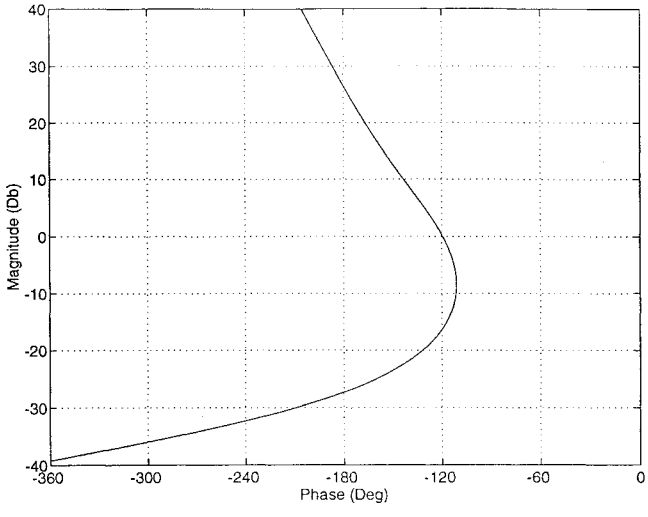

Fig. 4 Roll axis controller Nichols chart.

position vector and Earth's north pole as

$$A_{\text{com}} = [uvw]^T \tag{13}$$

where superscript T denotes the matrix transpose,

$$u = k \times r/|k \times r| \tag{14}$$

$$v = u \times r = (k \times r) \times r/|k \times r| \tag{15}$$

$$w = u \times v = -r \tag{16}$$

where w is the nadir vector, and

$$k = [0\ 0\ 1]^T \tag{17}$$

refers to Earth's north pole. The attitude error angles are given in terms of the commanded and estimated attitudes as the elements of the skew-symmetric matrix

$$\Theta_{\text{err}} = \tfrac{1}{2}\left[A_{\text{com}}(A_{\text{est}})^T - A_{\text{est}}(A_{\text{com}})^T\right] \tag{18}$$

The commanded rates are similarly given by the elements of the skew-symmetric matrix

$$\Omega_{\text{com}} = \frac{\mathrm{d}(A_{\text{com}})}{\mathrm{d}t}[A_{\text{com}}]^T \tag{19}$$

The rate errors are then the difference of the commanded rates and the estimated rates.

The control actuation is achieved with a set of four reaction wheels in a pyramidal arrangement providing redundant torque capability in all spacecraft axes. A standard proportional-integral-derivative (PID) controller is used to compute the reaction wheel torque commands (Fig. 3). The PID controller gains for each spacecraft axis K_P, K_I, and K_R are the following functions of the spacecraft's inertia I in that axis and the controller bandwidth ω_c chosen by the designer:

$$K_P = I(2\pi\omega_c)^2 \tag{20}$$

$$K_R = 0.707I(4\pi\omega_c) \tag{21}$$

$$K_I = 0.06436I(2\pi\omega_c)^3 \tag{22}$$

The moments of inertia used in the controller design are $I_{xx} = 2939$ kg · m^2, $I_{yy} = 1720$ kg · m^2, and $I_{zz} = 2900$ kg · m^2. The controller bandwidth was chosen to be 0.1 Hz to provide adequate spacecraft pointing performance and stability while avoiding the significant low-frequency flexible modes of the spacecraft. The controller is able to operate at a much higher bandwidth than the GOES-I controller because there is no need to filter out the large-magnitude noise of the GOES-I Earth sensor; this higher bandwidth improves performance and speeds the recovery from stationkeeping maneuvers. However, the controller will not excite the first significant flexible mode of the solar array, which is expected to be between 0.5 and 1.0 Hz.

Stability Analysis

The Interactive Controls Analysis (INCA) program was utilized to perform stability analysis of the proposed spacecraft controller. For the stability analysis the reaction wheels were modeled as a first-order lag, the spacecraft as a rigid body, and the DRIRU-II as a 15-Hz-bandwidth device with a second-order lag. Figure 4 is a Nichols chart of the roll axis controller showing an upper gain margin of 24 dB at 1.9 Hz and a lower gain margin of 26 dB at 0.02 Hz. The controller has 58 deg of phase margin at the gain crossover frequency of 0.16 Hz. These margins are deliberately chosen to be quite large at this point in the design because structural flexibility mode information is not available to be included in the plant dynamics model. The stability margins will decrease when a more complete flexible model of the spacecraft structure is included later in the spacecraft design process.

Spacecraft Motion Compensation

The spacecraft controller with its bandwidth of 0.1 Hz is capable of an impressive level of spacecraft line-of-sight pointing, but it is not capable of attenuating disturbances above that frequency. Figure 5 shows the approximate profiles of the expected GOES-N disturbance torques, which were used in developing the spacecraft motion compensation. The solar array stepping and blackbody calibration of the instrument mirrors exert the largest torques. The disturbances contain frequency components from below 0.1 Hz for part of the blackbody calibration to above 10 Hz for mirror scan motions. These disturbances require the spacecraft motion compensation system to attenuate disturbances of frequencies between the

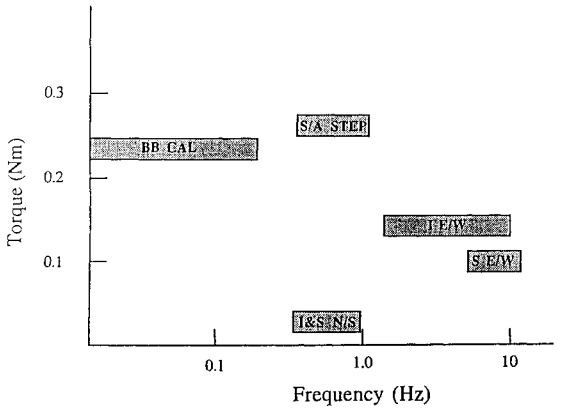

Fig. 5 Spacecraft disturbance torques: I, S, S/A, and BB CAL denote imager, sounder, solar array, and blackbody calibration, respectively.

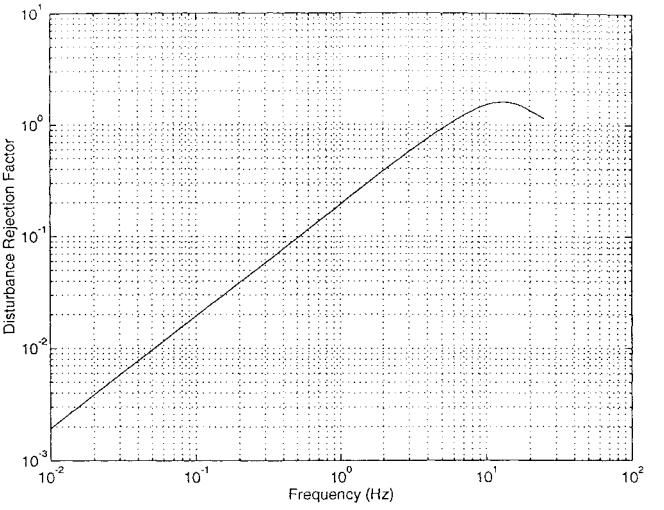

Fig. 7 Spacecraft motion compensation disturbance rejection.

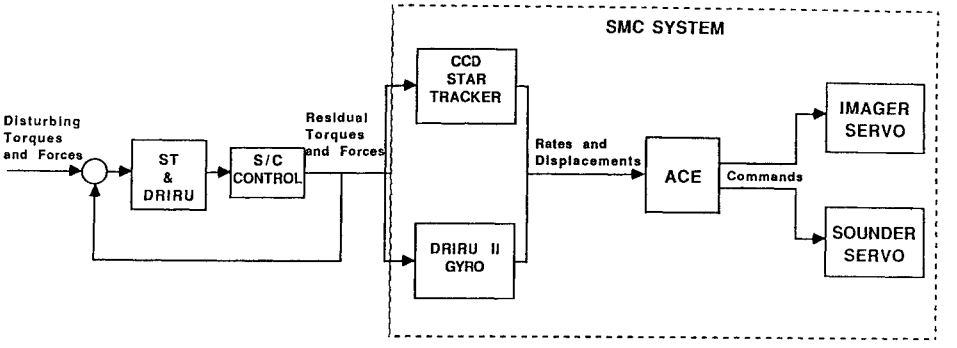

Fig. 6 Spacecraft motion compensation controller.

controller bandwidth and 5 Hz, since they would cause spacecraft jitter if unattenuated.

Compensation for disturbances at frequencies above 5 Hz is not required since the uncontrolled response to a given level of torque is inversely proportional to its frequency squared. If a Fourier component of the disturbance torque is given as

$$T = I\frac{\mathrm{d}^2\theta}{\mathrm{d}t^2} = K_T \sin \omega t \tag{23}$$

then integrating this twice gives

$$\theta = -K_T \sin \omega t / I\omega^2 \tag{24}$$

Obviously the higher frequency motions will not significantly disturb the rigid-body motion.

The spacecraft motion compensation senses the residual motion of the spacecraft by reading the gyros at the higher frequency of 50 Hz, providing more than three samples per period of an input at the gyro bandwidth frequency. Then the spacecraft motion compensation system calculates and feeds forward to the instrument servos a real-time gimbal correction to compensate for this motion, as illustrated in Fig. 6. Heritage for the spacecraft motion compensation comes from the Image Motion Compensation System developed for the ASTRO-1 payload on STS-35.[11,12]

The disturbance attenuation of the spacecraft motion compensation was estimated by rearranging the closed-loop transfer function of the east/west servo to form a transfer function of servo error response to attitude control electronics position correction command. Figure 7 depicts the disturbance rejection achieved by the spacecraft motion compensation. The gyro–star tracker pair supplies the gimbal correction at 50 Hz to the instrument servos, and the transfer function includes a lag due to the gyro dynamics and computational delay of the command signal. Disturbances are attenuated below a disturbance frequency of 5 Hz, and more than an order of magnitude performance improvement is achieved at 0.1 Hz.

Simulation

Simulation Models

The simulation uses a classical fourth-order Runge–Kutta integrator with fixed stepsize to integrate the equations of motion. The integration state has 26 components: 4 for the attitude quaternion, 3 for the total system angular momentum, 4 for the angular momenta of the reaction wheels, 3 for the gyro integrated error angles, 6 for the true spacecraft position and velocity, and 6 for the onboard computation of spacecraft position and velocity. The spacecraft equations of motion are the rigid-body equations as given, for example, in Ref. 10. The true and estimated spacecraft ephemerides are integrated using a force term consisting of Earth's mass and J_2, J_3, and J_4 oblateness terms, a nontrivial but not necessarily accurate orbit dynamics model. The force model constants and the initial conditions could be chosen separately for the true and onboard ephemerides, but they were identical for all the simulations presented here. The integration stepsize was taken to be 0.1 s, the gyro update interval, for simulations of the undisturbed motion. A smaller stepsize was used when imager and sounder disturbances were modeled, since these effects have variations on time scales shorter than 0.1 s.

At the beginning of the simulation, a fixed number of stars is randomly placed in the field of view of each star tracker. The positions of the stars are mapped into inertial space using the true star tracker alignment matrices and the true spacecraft attitude matrix, and a Gaussian error is placed on each inertial star vector to simulate the finite accuracy of star catalogs. As the simulation progresses, the fixed inertial star positions are mapped back into the tracker field-of-view coordinates using the true attitude and star tracker alignment matrices. The simulated star tracker measurements are two components of the star vector perpendicular to the tracker boresight with Gaussian noise added and quantization accounted for. Each star is

tracked until it leaves the tracker field of view, at which point another star is randomly placed in the field of view to keep a constant number of stars tracked.

The Kalman filter updates are based on the difference between the simulated and predicted star tracker measurements. The predicted measurements are computed in the same way as the simulated measurements, except that they use the estimated attitude and star tracker alignment matrices and are neither corrupted with noise nor quantized. The star tracker alignment knowledge was assumed to be perfect for all the results presented here. The estimated attitude quaternion is propagated with bias- and noise-corrupted gyro estimates of the spacecraft body rates (using the DRIRU-II gyro noise parameters) rather than the true body rates. The Kalman gain matrix is computed with constant process noise covariance and attitude state transition matrices assuming a constant negative pitch rate of one revolution per orbit. The simulated attitude control commands are based on the estimated attitude and rates, since the true attitude and rates are not known to the onboard computer. The command to each reaction wheel is limited to a maximum magnitude of 0.3 N · m and quantized to a least significant bit of 1.5×10^{-4} N · m, corresponding to a 12-bit wheel command.

Quiescent Registration Performance

Three different errors are of interest. The estimation error is the difference between the estimated attitude and the true attitude, the control error is the difference between the commanded attitude and the estimated attitude, and the pointing error is the difference between the commanded attitude and the true attitude. These errors are not independent, since the pointing error, the quantity of greatest significance, is the algebraic sum of the estimation error and the control error. The pointing error curve is always the smoothest of the three curves, since neither the true attitude nor the commanded attitude contains the high-frequency sensor noise appearing in the estimated attitude. This smoothness property can be used to distinguish the

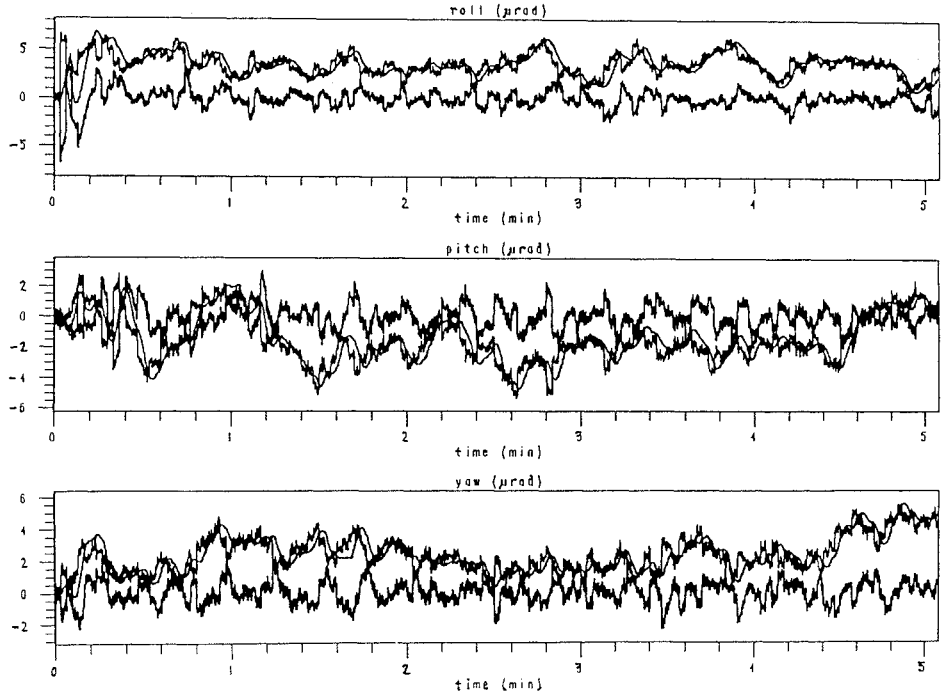

Fig. 8 Attitude estimation errors.

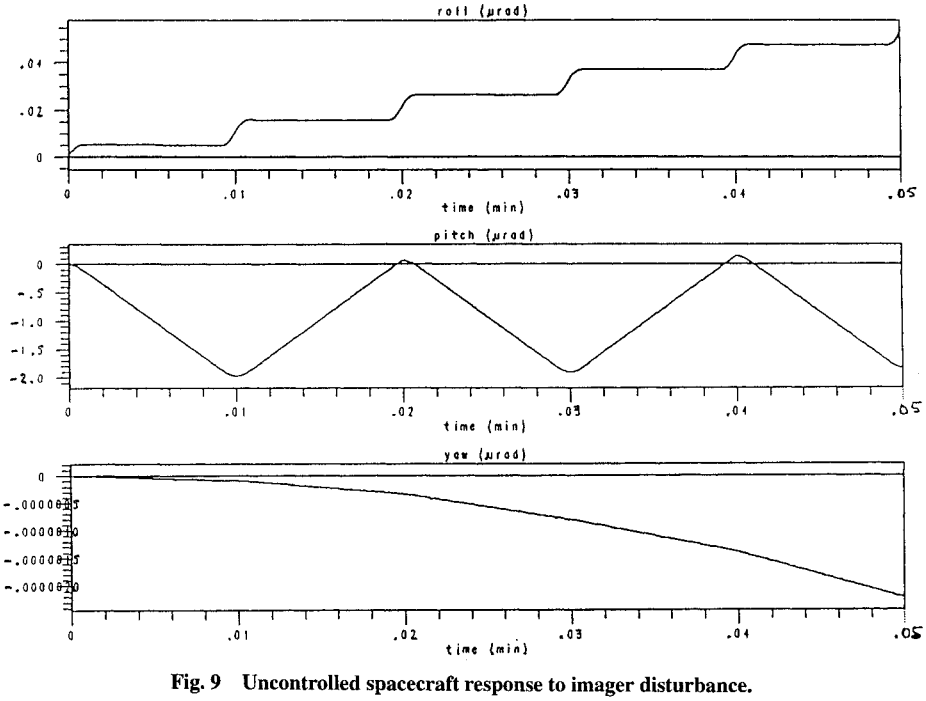

Fig. 9 Uncontrolled spacecraft response to imager disturbance.

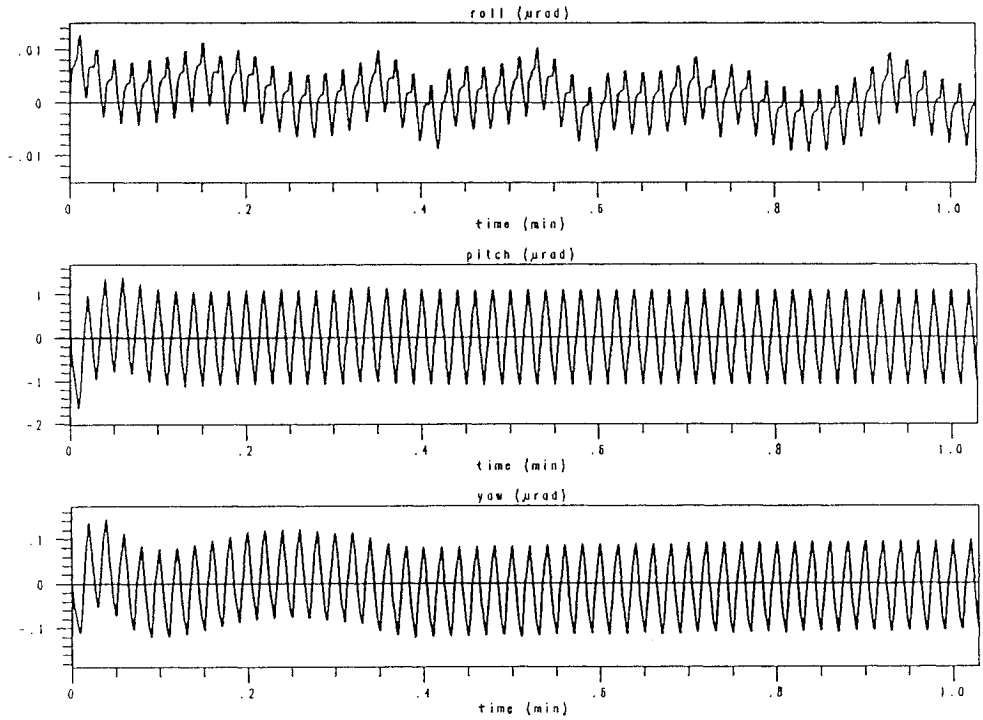

Fig. 10 Controlled spacecraft response to imager disturbance.

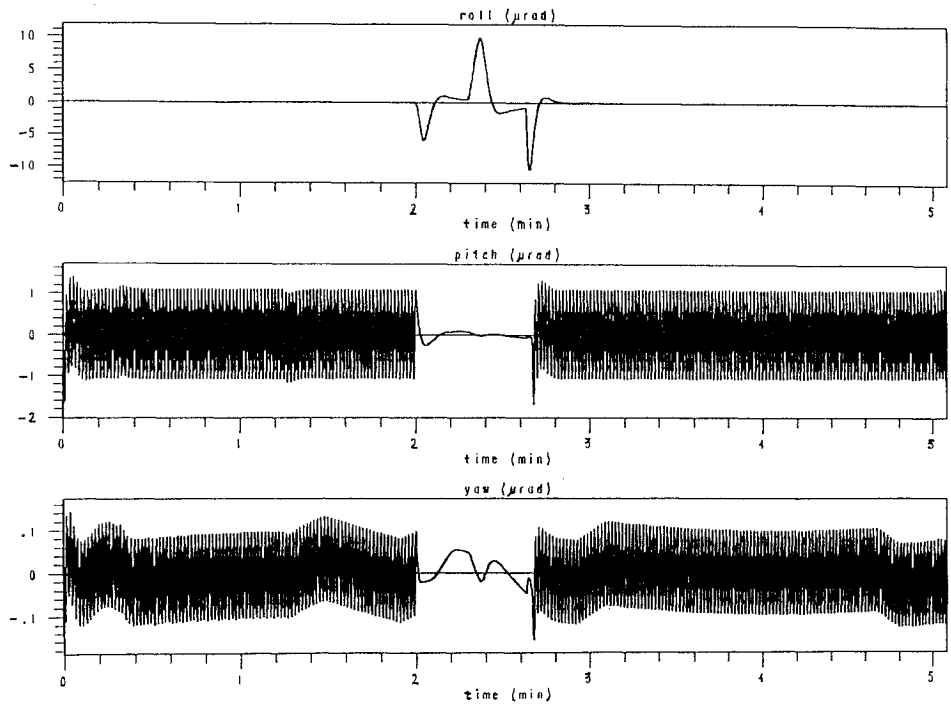

Fig. 11 Controlled spacecraft response to imager disturbance with blackbody calibration slew.

pointing error curve from the other error curves. In Fig. 8, the control error curve is always the curve that stays closest to the horizontal axis, since the estimation errors are always larger than the control errors. When only two curves can be distinguished, it is because the estimation error and pointing error plots are too close to be resolved.

Figure 8 shows the best estimate of the performance achievable with currently available star trackers. This estimate assumes a 14.5 μrad noise equivalent angle and a 16-bit star tracker data word, giving a least significant bit of 2.13 μrad. There were assumed to be five stars in each tracker field of view, and the star catalog errors were 5 μrad on each axis perpendicular to the line of sight. These errors are taken to represent the combined effect of actual catalog errors and calibration errors. The latter are hard to model more accurately, since they are neither random nor constant for a given star. The Kalman filter update interval was set at 1 s, well within the capabilities of both the star trackers and the onboard processor. The curves show attitude standard deviation of about 1.7 μrad on each axis.

Spacecraft Disturbance Accommodation

This section shows the simulated response of the control system to imager and sounder disturbances. The controlled attitude errors resulting from the sounder disturbances are extremely small, never exceeding 0.1 μrad, so the sounder disturbance is negligible in the absence of blackbody calibration slews. Since the disturbance profiles of imager and sounder blackbody slews are identical, only the response to imager disturbances will be discussed in detail.

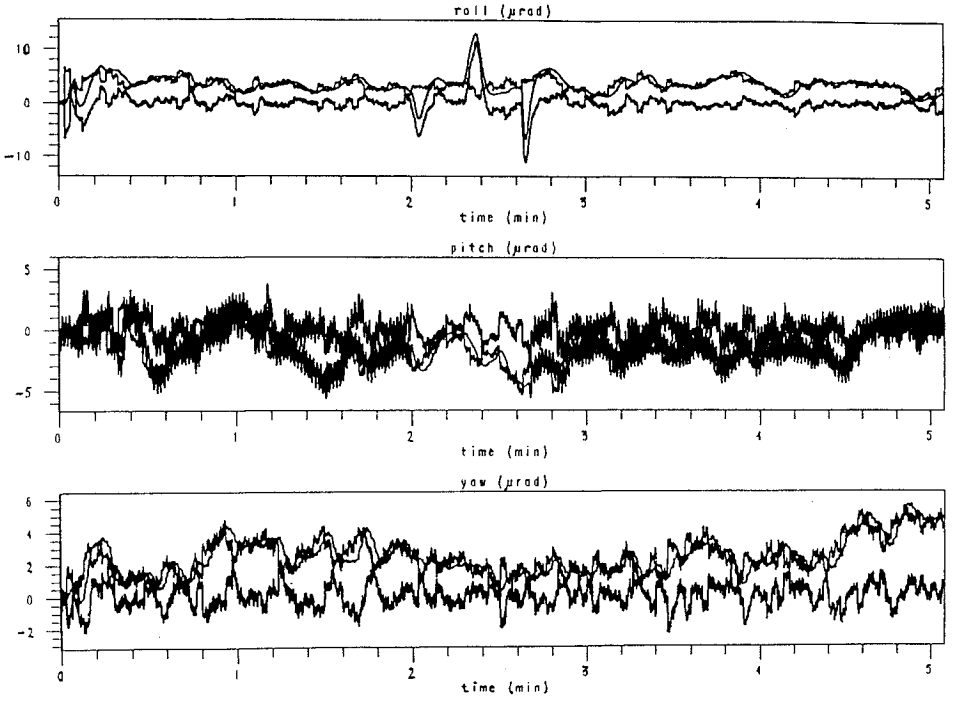

Fig. 12 Combined response to estimation errors and imager disturbance with blackbody calibration slew.

The imager scan time was set to 0.6 s, giving a scan length of approximately 6 deg, allowing for mirror acceleration and deceleration. The same three error curves are plotted as for the quiescent registration performance. The simulations shown in Figs. 9–11 were made with zero initial attitude estimation errors and perfect gyros to exhibit the performance of the controller not masked by estimation errors. In these runs, the Kalman update time was set to a time longer than the length of the simulation, since star references are not needed if the initial attitude estimate and the gyros are perfect. Also in these runs the estimation error is zero and the pointing and control errors are equal to one another. Thus only two curves are visible on each plot, one of which lies exactly on the horizontal axis. Figure 9 shows the uncontrolled spacecraft response to the imager east/west scan (about the roll axis) and north/south step (about the pitch axis). The off-diagonal elements of the spacecraft moment-of-inertia tensor were set equal to zero in this simulation, so the roll-yaw coupling is due to the 1-revolution-per-orbit pitch motion. Figure 10 shows the controlled response with perfect attitude estimation on a different time scale. This and all following runs used the full moment-of-inertia tensor, so the roll motion shows the combination of the direct response to the north/south steps and the coupling of the east/west scan through the xy product of inertia. Figure 11 is the same case as Fig. 10 except that a longer time span is shown, including a blackbody calibration at 2 min. The blackbody calibration gives a large attitude disturbance, as expected, with pointing errors as large as 10 μrad. Figure 12 shows the combined effect of estimation errors and imager disturbances; the estimation error, control error, and pointing error are all nonzero in this run. Comparison of Figs. 8 and 12 shows that the estimation errors dominate the control errors except during the blackbody calibration maneuver, as expected.

Spacecraft Motion Compensation

The above simulations show that the control errors are about 1 μrad except during blackbody calibration slews, at which times they are as large as 10 μrad, as measured by maximum deviations from zero. The control errors can further be reduced by spacecraft motion compensation, whereas the estimation errors cannot, since they are unknown to the controller. Figure 13 shows the enhanced disturbance rejection of the GOES-N spacecraft with the spacecraft motion compensation capability for jitter at the instrument focal plane. The instrument line-of-sight pointing error during a blackbody calibration slew is reduced by the spacecraft controller to 10 μrad from

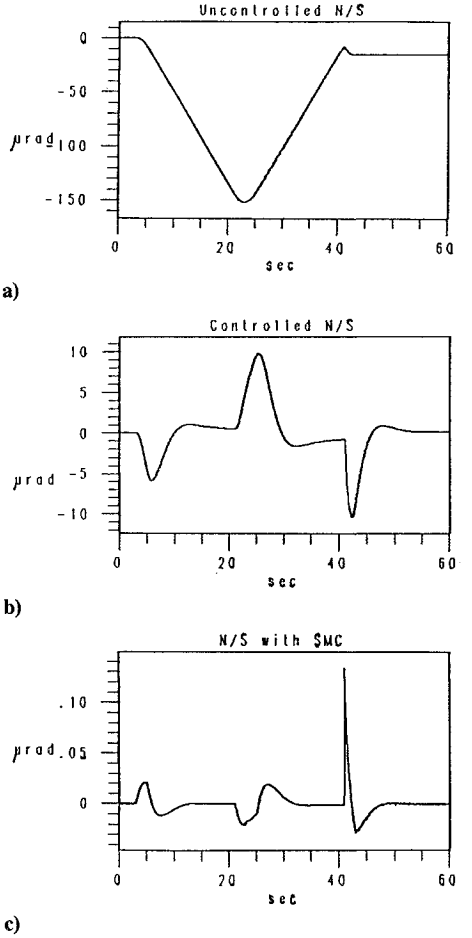

Fig. 13 Spacecraft motion compensation, north/south scan.

the uncontrolled value of 150 μrad and then is further reduced by spacecraft motion compensation to the acceptable level of 0.1 μrad. Thus the effective overall performance with spacecraft motion compensation in the presence of attitude disturbances is the same as in the quiescent case, with pointing errors of 1.7 μrad (1σ) per axis.

Conclusions

Aside from its increased performance, the attitude control system employing a three-axis inertial reference unit and three star trackers has several advantages over an Earth sensor-based momentum bias system for geostationary applications. The four reaction wheels for this option are lighter than the two momentum wheels and one reaction wheel used in the momentum bias system. Simpler horizon sensors are needed for acquisition and safehold operations than would be required for fine pointing. Deletion of the deployable solar sail used to compensate for solar radiation pressure torques in the momentum bias system alleviates instrument cooling problems while reducing cost, weight, volume, and risk. The risk is very low for the recommended system. Tuned rotor inertial reference units have been employed on several missions with great success. CCD star trackers had not been space tested at the time of this design study, but they are based on proven technology and should be well tested long before they are needed for this application. The algorithms for combining the gyro and star tracker data have been extensively tested in space, and the data system required for these computations is well within the bounds of current technology.

Simulations of the proposed attitude control system show control errors having maximum deviations from zero of about 1 μrad except during calibration slews of the instrument mirrors, at which times they are as large as 10 μrad. The sensor line-of-sight pointing errors are reduced to 0.1 μrad by spacecraft motion compensation, a very effective method for enhancing instrument pointing performance with minimal impact on the spacecraft system, requiring no additional sensors and minimal increase in computational burden. The dominant error is then the uncorrectable attitude estimation error with standard deviation of approximately 1.7 μrad per axis, well within the budgeted error of 14 μrad (3σ).

References

[1]Murrell, J. W., "Precision Attitude Determination for Multimission Spacecraft," AIAA Paper 78-1248, Aug. 1978.

[2]Markley, F. L., "Attitude Control Algorithms for the Solar Maximum Mission," AIAA Paper 78-1247, Aug. 1978.

[3]Rose, E. F., and Berkery, E. A., "On-Orbit Control System Performance of the HEAO-2 Observatory," *Journal of Guidance, Control, and Dynamics*, Vol. 4, 1981, pp. 148–156.

[4]Lefferts, E. J., Markley, F. L., and Shuster, M. D., "Kalman Filtering for Spacecraft Attitude Estimation," *Journal of Guidance, Control, and Dynamics*, Vol. 5, No. 5, 1982, pp. 417–429.

[5]Markley, F. L., Bauer, F. H., Deily, J. J., and Femiano, M. D., "Attitude Control System Conceptual Design for the GOES-N Spacecraft Series," AIAA Paper 91-2832, Aug. 1991.

[6]McQuerry, J. P., Radovich, M. A. Jr., and Deters, R. A., "A Precision Star Tracker for the Nineties: A System Guide to Applications," AAS Paper 90-014, Feb. 1990.

[7]Stanton, R. H., Alexander, J. W., Dennison, E. W., Glavich, T. A., Salomon, P. M., and Williamson, R. E., "ASTROS: A Sub-Arcsec CCD Star Tracker," *State-of-the-Art Imaging Arrays and their Applications*, edited by K. N. Prettyjohns, Proceedings of the SPIE 501, 1984, pp. 256–282.

[8]Stanton, R. H., Alexander, J. W., Dennison, E. W., Glavich, T. A., and Hovland, L. F., "Optical Tracking Using Charge-Coupled Devices," *Optical Engineering*, Vol. 26, No. 9, 1987, pp. 930–938.

[9]Farrenkopf, R. L., "Analytic Steady-State Accuracy Solutions for Two Common Spacecraft Attitude Estimators," *Journal of Guidance, Control, and Dynamics*, Vol. 1, No. 4, 1978, pp. 282–284.

[10]Wertz, J. R. (ed.), *Spacecraft Attitude Determination and Control*, Reidel, Boston, MA, 1978.

[11]Bauer, F. H., and Deily, J. J., "Image Motion Compensation for the Ultraviolet Imaging Telescope," AIAA Paper 90-3246, Aug. 1990.

[12]Deily, J. J., and Bauer, F. H., "Flight Performance of a Shuttle-Based Image Motion Compensation System for the Ultraviolet Imaging Telescope," AIAA Paper 91-2622, Aug. 1991.